



Driver Sleepiness Detection Using LSTM Neural Network

Yini Deng¹, Yingying Jiao¹, and Bao-Liang Lu^{1,2,3}(✉)

¹ Center for Brain-like Computing and Machine Intelligence, Department of Computer Science and Engineering, Shanghai Jiao Tong University, Shanghai, China
dengyini@sjtu.edu.cn, jiaoyingying2010@163.com

² Key Laboratory of Shanghai Education Commission for Intelligent Interaction and Cognition Engineering, Shanghai Jiao Tong University, Shanghai, China

³ Brain Science and Technology Research Center, Shanghai Jiao Tong University, Shanghai, China
bllu@sjtu.edu.cn

Abstract. Driver sleepiness has become one of the main reasons for traffic accidents. Previous studies have shown that two alpha-related phenomena - alpha blocking phenomenon and alpha wave attenuation-disappearance phenomenon - respectively represent two different sleepiness levels: the relaxed wakefulness and the sleep onset. Thus, we proposed a novel model to detect those two alpha-related phenomena based on EEG and EOG signals so as to determine sleepiness level. EOG and EEG signals inherently have temporal dependencies, and the sleepiness level transition is also a temporal process. Correspondingly, continuous wavelet transform represents physiological signals well, and LSTM is capable of handling long-term dependencies. Thus, our proposed detection model utilized continuous wavelet transform and LSTM neural network for detecting driver sleepiness. The performance of our detection model are twofold: the recall and precision for detecting start and end points of alpha waves are generally high, and the LSTM classifier reaches a mean accuracy of 98.14%.

Keywords: Driver sleepiness detection · EEG · EOG
Continuous wavelet transform · LSTM

1 Introduction

Lacking sleeping, numerous drivers have reported that they actually fell asleep while driving [10]. This phenomenon indicates that some drivers tend to ignore the early signs of drowsiness, and are consequently unaware of the following period of sleep onset [1, 7]. Therefore, developing a reliable method to evaluate driver sleepiness is of urgent need and of great importance.

Although there are many ways to evaluate sleepiness level, such as self evaluation and vehicle-based evaluation, using physiological signals to detect driver sleepiness is one of the most reliable ways [2, 12]. Shabani *et al.* used RQA of

EEG to differentiate alert to drowsy with 90.6% accuracy [11]. From our previous research, a new alpha wave attenuation-disappearance phenomenon has been proven to be a general pattern for predicting the entry of sleep during simulated driving in daytime [8]. Besides this phenomenon, we also observed the typical alpha blocking phenomenon in the simulated driving process. According to [4, 5], it refers to the alpha rhythm activity which appears when eyes are closed under the relaxed wakefulness, and it disappears when eyes are reopened. Thus, alpha blocking phenomenon and alpha wave attenuation-disappearance phenomenon represent two different sleepiness levels: the relaxed wakefulness and the sleep onset.

In our previous work, we combined continuous wavelet transform with SVM to detect two different alpha-related phenomena [9]. However, the sleepiness level transition is a temporal process, and physiological signals like EOG have inherent temporal dependencies [14]. Our previous model didn't take temporal information into account. Thus, we introduced LSTM network to deal with those temporal dependencies in this paper. Being a special form of recurrent neural networks, LSTM has the ability to capture temporal dependency property. And it has achieved great successes in the field of machine translation and speech recognition. Meanwhile, continuous wavelet transform represents physiological signals well. Therefore, we proposed a novel model based on continuous wavelet transform and LSTM network to detect the change of alpha waves and to distinguish those two alpha-related phenomena.

2 Two Experiments and Their Settings

We conducted two different types of experiments for each subject: the eye-closure experiment and the simulated driving experiment. These two experiments aim to obtain EEG and EOG signals under two different sleepiness levels: the relaxed wakefulness and the sleep onset. In total, 12 healthy subjects (4 females and 8 males with an average age of 22) who have siesta habit for more than a year were recruited from Shanghai Jiao Tong University (Fig. 1).

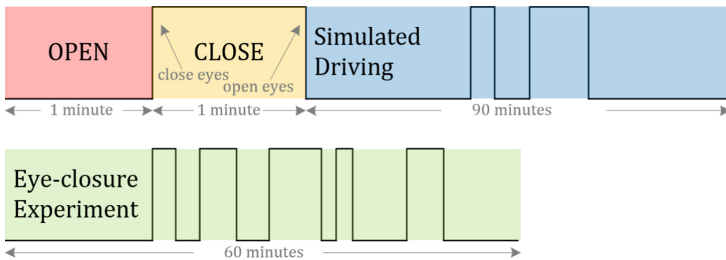


Fig. 1. Procedures for simulated driving experiments and eye-closure experiments

2.1 Eye-Closure Experiment

This experiment aims to obtain the subject's EEG and EOG signals under the relaxed wakefulness. The subject closed and opened his/her eyes according to our instructions, and only alpha blocking phenomenon appeared during the eye closure period.

Every subject participated in the eye-closure experiment once, and the experiment lasted for 60 min. We can get an averaged 250 periods of closing and reopening eyes from it. A portion of the data obtained from this experiment was used as the training data.

2.2 Simulated Driving Experiment

This experiment aims to induce the sleepiness level change of the subject from relaxed wakefulness to sleep onset during a simulated driving process. In this experiment, we can observe both alpha blocking phenomenon and alpha wave attenuation-disappearance phenomenon.

Every subject participated in the simulated driving experiment during the siesta time, and the experiment lasted for about 90 min. When the experiment began, the subject first kept the eyes closed and opened for one minute respectively. We defined those two periods as CLOSE and OPEN, which were used to calculate wavelet energy threshold later. Then, the subject started to do simulated driving. If a subject's higher sleepiness level was not induced during the experiment, the subject would participate in this experiment again.

2.3 Data Recording

As shown in Figs. 2 and 3, we used 6 electrodes to obtain EEG and EOG signals, including one reference electrode and one ground electrode placed behind the ears, two occipital EEG electrodes (O1 as an alternative if O2 is noisy), two EOG electrodes (Vu and Vd) placed above and under the left eye. All the signals were recorded at an 1000 Hz sampling rate using ESI NeuroScan System. Meanwhile, a camera was placed behind the steering wheel to monitor the state of the subject. The video from the camera and the signals displayed on Scan software window were synchronously recorded into a file, so that we can review after the experiment and investigate the relevance between eye movements and EEG or EOG signals.

3 Driver Sleepiness Detection Model

The purpose of our detection model is to track the change of alpha waves in O2 signal and to detect two alpha-related phenomena based on this change, so that we can detect driver sleepiness. We used offline processing to simulate the real-time driver sleepiness detection on signals from simulated driving experiments, and the sliding window was the key to our simulation. As depicted in Fig. 4, we first utilized a sliding window to calculate alpha wavelet energy threshold E_{th}

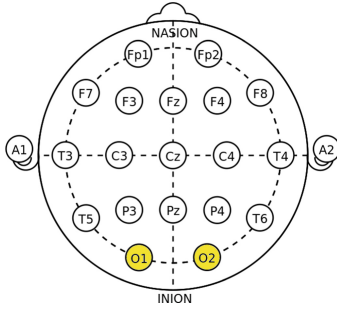


Fig. 2. EEG electrode placement

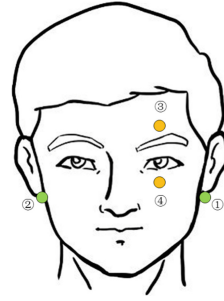


Fig. 3. EOG electrode placement

on O2 signal during CLOSE and OPEN periods. Then, E_{th} was used to detect the start and end points of alpha waves on O2 signal from the simulated driving process, whose alpha wavelet energy was also calculated using a sliding window. If the detected point was an end point, we extracted features from its corresponding VEOG signal and put those features into the trained LSTM classifier. Finally, the classifier determined whether the detected end point was the end point of alpha waves in alpha blocking phenomenon or alpha wave attenuation-disappearance phenomenon.

In terms of the training of the LSTM classifier, we used VEOG signals from the two experiments as the training data. The detection of end points was sensitive to the alpha wavelet energy threshold E_{th} : the detected end point might deviate from the actual end point. Thus, we utilized LSTM network so that it could take information from previous sequences into account, yielding a better classification performance.

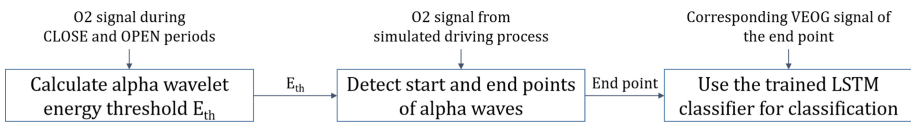


Fig. 4. The flowchart of the detection model

3.1 Visual Marking for Two Alpha-Related Phenomena

As mentioned in [9], an eye closure event (ECE) was defined as the period between the end of the upward trend line caused by closing eyes and the end of the downward trend line caused by reopening eyes in VEOG signal. In Fig. 5, we can see that two kinds of eye closure events, ECE^1 and ECE^2 , exist alternately in simulated driving experiments.

ECE^1 is the eye closure event corresponding to alpha blocking phenomenon. This phenomenon refers to the alpha rhythm activity which appears when eyes

are closed and disappears when eyes are reopened, indicating the relaxed wakefulness. In Fig. 5, experts visually marked the start point s^1 and the end point e^1 of alpha waves on O2 signal, and this continuous alpha wave represents alpha blocking phenomenon. Those two points are equivalent to the start point and end point of ECE^1 on VEOG signal.

ECE^2 is the eye closure event corresponding to alpha wave attenuation-disappearance phenomenon. The visually marked split point p^2 divides ECE^2 into two phases: alpha wave attenuation phase and alpha wave disappearance phase. When the subject closes his/her eyes, the amplitude of alpha waves on O2 signal attenuates until alpha waves disappear. This phenomenon indicates the sleep onset, which means the subject has a high sleepiness level. Experts also marked the start point s^2 and end point p^2 of alpha waves in the alpha attenuation phase on O2 signal. Those two points are equivalent to the start point and split point of ECE^2 on VEOG signal. Besides, similar to the marking of end point e^1 in ECE^1 , the end point of ECE^2 on VEOG signal was also visually marked according to the downward trend line.

Therefore, the two different alpha-related phenomena have different representations on O2 and VEOG signals, and indicate two different sleepiness levels.

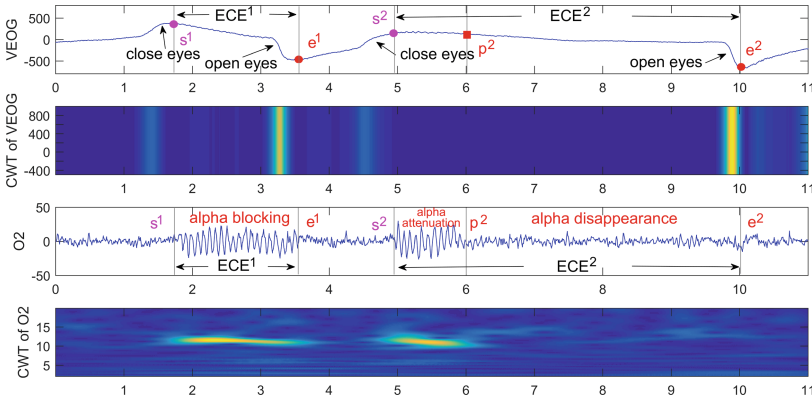


Fig. 5. Visual marks for two different alpha wave phenomena

3.2 Calculating Alpha Wavelet Energy Threshold E_{th}

Similar to the feature extraction method in [9], continuous wavelet transform (CWT) was applied to O2 signal during OPEN and CLOSE periods in simulated driving experiments to calculate wavelet threshold E_{th} . Complex Morlet wavelet was selected to do CWT because it is geometrically similar to alpha waves. We picked the scales corresponding to alpha frequency band ($F = [8,12]$ Hz) from range $[1, 1024]$. Wavelet energy $w(t)$ was thus calculated according to wavelet coefficients on those scales and was further averaged in time window T . Here, T was set to 1 s, and the sliding step of the time window was set to 0.1 s. Thus, we

got numerous 1 s alpha wavelet energy values for OPEN and CLOSE periods, respectively. E_{th} is the mean of alpha wavelet energy distribution’s minimum during CLOSE period and its maximum during OPEN period.

3.3 Detecting Start and End Points of Alpha Waves

E_{th} was used to detect the start and end points of alpha waves on O2 signal, and it was calculated for each subject. We used Complex Morlet wavelet to do CWT on O2 signal of the testing data. As mentioned in 3.2, the time window length was set to 1 s, and the sliding offset was 0.1 s. Thus, we can get an alpha wavelet energy curve on O2 signal, as depicted in Fig. 6. As soon as the current wavelet energy was higher than E_{th} , the current time point was considered as the start point s' of alpha waves. Afterwards, if the wavelet energy was continuously higher than E_{th} , these time points were the proof for the persistent presence of alpha waves. Until the wavelet energy was lower than E_{th} , the current time point was the end point of alpha waves.

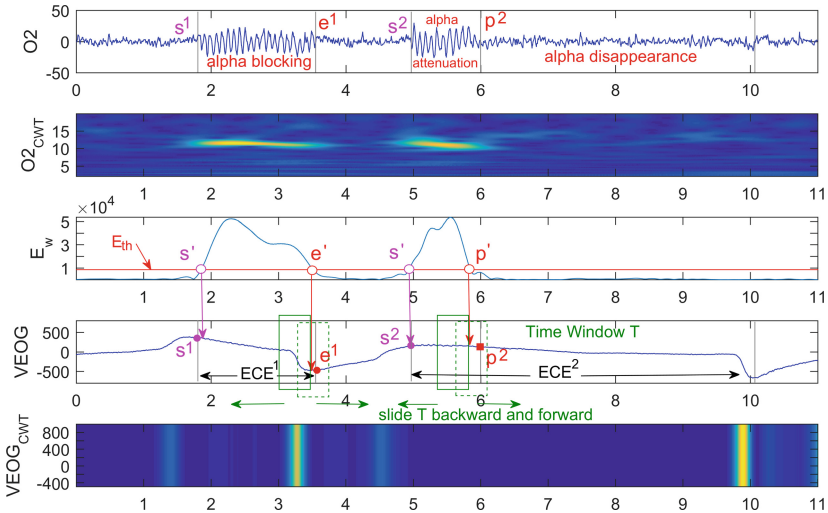


Fig. 6. Wavelet energy curve of O2 signal

3.4 LSTM Classifier

The key to distinguishing the two types of alpha-related phenomena is to differentiate the end point e^1 in ECE^1 from the split point p^2 in ECE^2 . Thus, we defined e^1 as negative, and p^2 as positive. Besides, We used a leave-one-subject-out cross validation method, which took data from 11 subjects as the training data, and the remaining one subject as the testing data.

Feature Extraction of VEOG Signals. We used Haar wavelet to do CWT for VEOG signals, which is similar to the method used in [9], because its mother wavelet has a similar shape to the waveform in VEOG signals. CWT with Haar wavelet scaling from 1 to 128 was applied to the 0.5 s VEOG signal, which was either $[e^1 - 0.5 \text{ s}, e^1 \text{ s}]$ or $[p^2 - 0.5 \text{ s}, p^2 \text{ s}]$. As the LSTM classifier has the sequence length concept, the 0.5 s time window was moved forward for 0.125 s and 0.25 s, and backward for 0.125 s and 0.25 s. Finally, we can get five 128-dimensional Haar wavelet feature vectors for each training sample, corresponding to the sequence length 5 of the LSTM classifier. When labeling the training data, we labeled all 5 feature vectors for each p^2 as positive and those for each e^1 as negative.

LSTM Neural Networks. As the input features have temporal dependencies, we introduced Long Short Term Memory (LSTM) neural network to incorporate this information [6]. Being an RNN using LSTM cells, LSTM neural network is capable of preventing vanishing gradient problems [3]. Moreover, in practice, LSTM neural networks handle long-term dependencies well. Cell state C_t , which is propagated over time, is the key to LSTM neural networks. At every time step, C_t is updated as follows:

$$\begin{aligned} f_t &= \sigma(W_f \cdot [h_{t-1}, x_t] + b_f) \\ i_t &= \sigma(W_i \cdot [h_{t-1}, x_t] + b_i) \\ \tilde{C}_t &= \tanh(W_C \cdot [h_{t-1}, x_t] + b_C) \\ C_t &= f_t * C_{t-1} + i_t * \tilde{C}_t \end{aligned} \quad (1)$$

where x_t is the current input, h_{t-1} is the previous output of the LSTM network, f_t and i_t denote the forget gate and the input gate, respectively, \tilde{C}_t denotes the candidate value, W_f , W_i and W_C are weight matrices, b_f , b_i and b_C are biases, and σ is the sigmoid function.

The forget gate controls the information to be thrown away from the cell state, while the input gate decides the information to be stored in the cell state. Then, we can get the output of LSTM blocks as follows:

$$\begin{aligned} o_t &= \sigma(W_o \cdot [h_{t-1}, x_t] + b_o) \\ h_t &= o_t * \tanh(C_t) \end{aligned} \quad (2)$$

where o_t denotes the output gate, and W_o and b_o are weight matrix and bias, respectively. So, h_t is a filtered version of the cell state, regulated by the output gate.

Our classification model is depicted in Fig. 7. Dropout is applied to the output of LSTM layer, so that the model is more robust. After that, there is one classification layer, which uses hinge loss with L2-regularization as the objective loss function. Therefore, we can consider it as a linear kernel SVM [13].

3.5 Using the LSTM Classifier for Classification

When an end point of alpha waves was detected, we found its corresponding point on VEOG signal and utilized Haar wavelet to do CWT. As mentioned in Sect. 3.4,

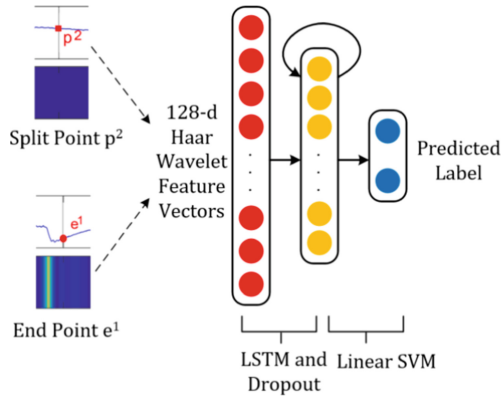


Fig. 7. LSTM classifier

five 128-dimensional feature vectors were extracted. They were further put into the LSTM classifier to determine whether this end point is the end point e' of ECE^1 or the split point p' of ECE^2 . This is equivalent to determining whether this end point is the end point of alpha waves in alpha blocking phenomenon or in alpha wave attenuation-disappearance phenomenon.

Actually, we get one label, which is the bigger one in the two output labels, for each of the five feature vectors in the input sequence, while we only need one label to determine whether the detected end point is the end point of alpha waves in alpha blocking phenomenon or in alpha wave attenuation-disappearance phenomenon. To solve this nonuniformity, we design a mapping function to map the five output labels to one final label. That is, we choose the label which is the most frequent among the five output labels as the final label of the detected end point.

4 Experimental Results

4.1 Training Details

For the training of the classifier, we used data from the two experiments of the 11 subjects. According to our observation, there were very few eye closure events during the early stage of the simulated driving experiment. During the late stage, as the subject became more sleepy, ECE^1 and ECE^2 appeared alternately and frequently. Thus, for each subject, we picked a 30-min period from the late stage of his/her simulated driving experiment. Besides, due to the approximately balanced amount of e^1 and p^2 in simulated driving experiments, we only marked part of the e^1 in eye-closure experiments as negative, so that the whole training set wouldn't be significantly unbalanced. After the training of the LSTM classifier, the whole model was tested on the simulated driving experiment from the one subject which was left out. And we used the averaged result to evaluate our model.

Training the LSTM Classifier. The whole classifier network was trained using Adam optimizer. For each training and testing set, we randomly selected tens of sets of hyper-parameters within a given range to train the model. As shown in Table 1, the hyper-parameters include the size of the hidden layer, the dropout probability, the L2 regularization strength and the learning rate. 10-fold cross validation was used to choose the best set of hyper-parameters.

Table 1. The hyper-parameters and their range of the LSTM classifier

Hyper-parameter	Range
Hidden size	16 ~ 128
Dropout probability	0.2 ~ 0.9
\log_{10} (L2 regularization strength)	-7 ~ -2
\log_{10} (learning rate)	-5 ~ -1

Training SVM and k -NN. For linear SVM, we used sklearn package in Python to do the training, and adjusted the parameter C to achieve the best performance. For k -NN, we set k to 1, because it had the best performance in the range [1, 5] on our training data.

4.2 Performance of Detecting Alpha Wave Start and End Points

If the detected start point s' or end point e' fell into the range of $[s^1(s^2) - 0.5 \text{ s}, s^1(s^2) + 0.5 \text{ s}]$ or $[e^1 - 0.5 \text{ s}, e^1 + 0.5 \text{ s}]$, the point was considered as a correctly detected point by the model. Similarly, if the detected split point p' fell into the range of $[p^2 - 0.8 \text{ s}, p^2 + 0.8 \text{ s}]$, it was considered as a correctly detected point. Due to the greater subjective bias for marking the split point, we defined a larger time range of 0.8 s.

To evaluate how well our detection model detects the start and end points of alpha waves, we introduced True Positive (TP), False Positive (FP) and False Negative (FN) to show the performance of detecting start and end points of alpha waves. Here, TP and FP referred to the number of start and end points that were correctly detected and wrongly detected, while FN was the number of those which were visually marked but not detected by the model. Meanwhile, recall, precision and F1 score were used to investigate the performance of detecting start and end points. From Table 2, we can see that the recall, precision and F1 score for detecting start and end points of ECE^1 are generally high across different subjects with mean values of 96.3%, 93.9%, 95.2% and 95.0%, 95.1%, 94.8%, respectively. Similarly, those three metrics for detecting start and split points of ECE^2 are also generally high with mean values of 96.0%, 95.7%, 95.8% and 94.5%, 94.3%, 94.6%, respectively, as shown in Table 3.

Table 2. ECE^1 detection performance

Subject	# ECE^1	Start point			End point		
		Recall (%)	Precision (%)	F1 (%)	Recall (%)	Precision (%)	F1 (%)
1	34	94.1	97.0	95.5	100.0	97.1	98.6
2	28	100.0	96.6	98.2	96.4	93.1	94.7
3	22	100.0	91.3	95.5	90.9	95.2	93.0
4	20	95.0	82.6	88.4	95.2	90.9	93.0
5	26	100.0	96.3	98.1	92.3	92.3	92.3
6	28	92.9	89.7	91.2	89.3	96.2	92.6
7	28	100.0	96.6	98.2	96.4	100.0	98.2
8	27	96.3	92.9	94.5	96.3	92.9	94.5
9	23	95.7	95.7	95.7	91.3	95.5	93.3
10	21	90.5	100.0	95.0	95.2	100.0	97.6
11	25	96.0	96.0	96.0	100.0	92.6	96.2
12	26	100.0	92.9	96.3	92.3	96.0	94.1
Mean \pm SD		96.3 ± 3.0	93.9 ± 4.6	95.2 ± 2.8	95.0 ± 3.7	95.1 ± 2.9	94.8 ± 2.2

Table 3. ECE^2 detection performance

Subject	# ECE^2	Start point			Split point		
		Recall (%)	Precision (%)	F1 (%)	Recall (%)	Precision (%)	F1 (%)
1	24	100.0	96.0	98.0	100.0	92.3	96.0
2	35	100.0	100.0	100.0	97.1	97.1	97.1
3	30	93.3	96.6	94.9	96.7	96.7	96.7
4	27	88.9	92.3	90.6	85.2	92.0	88.5
5	24	95.8	95.8	95.8	95.8	100.0	97.9
6	26	92.3	92.3	92.3	92.3	88.9	90.6
7	27	96.3	92.9	94.5	88.9	96.0	92.3
8	28	100.0	90.3	94.9	100.0	93.3	96.6
9	26	96.2	100.0	98.0	96.2	89.3	92.6
10	23	100.0	95.8	97.9	95.7	95.7	95.7
11	29	96.6	100.0	98.2	93.1	96.4	94.7
12	28	92.9	96.3	94.5	92.9	100.0	96.3
Mean \pm SD		96.0 ± 3.6	95.7 ± 3.2	95.8 ± 2.7	94.5 ± 4.3	94.3 ± 3.4	94.6 ± 2.9

4.3 Comparison of Three Classifiers

To make the comparison simpler, we only took into account those end points which were correctly detected by the detection models. As shown in Table 4, the LSTM classifier achieves the best accuracy of 98.14% among the three classifiers, and it has the smallest standard deviation of 0.75%, which makes it more robust. In contrary, k -NN is the worst at doing classification, and it is the most unstable one. Although the mean accuracy of linear SVM is close to that of the LSTM

classifier, its performance is unstable across different subjects. We think the stableness of the LSTM classifier owes to its recurrent structure which uses information from previous sequences to do classification. Even if the information carried in one of the 5 input feature vectors is incomplete or inaccurate, the classifier is able to give the correct label with the help of temporal information. Meanwhile, if the detected end point deviates slightly from the visually marked end point, the vital part around the end point can still fall into the range of the five sliding windows in LSTM. This ability of integrating all the information in previous sequences makes LSTM better at classifying the end points.

Table 4. Accuracies and standard deviations of different classifiers

Subject	k-NN	SVM	LSTM
1	90.34	93.44	96.90
2	86.56	95.74	98.03
3	86.53	95.92	98.78
4	90.70	97.21	98.14
5	85.11	95.74	97.87
6	87.76	96.33	99.18
7	89.80	92.16	98.43
8	90.74	92.96	96.67
9	93.48	95.22	97.83
10	92.86	95.71	98.57
11	88.85	95.77	98.46
12	89.60	94.80	98.80
Average accuracy	89.35	95.08	98.14
SD	2.54	1.49	0.75

5 Conclusion

In this paper, we have introduced a driver sleepiness detection model to detect the change of alpha waves and classify two different alpha-related phenomena. This method utilized continuous wavelet transform to extract features from EEG and EOG signals, and used an LSTM classifier to do classification based on temporal information. The experimental result indicates that the recall, precision and F1 score for detecting start and end points of alpha waves are generally high. Meanwhile, the proposed LSTM classifier achieves a mean accuracy of 98.14%. Thus, our proposed method, which places few electrodes on subjects and has satisfying results, is both feasible and practical for detecting driver sleepiness.

Acknowledgments. This work was supported in part by the grants from the National Key Research and Development Program of China (Grant No. 2017YFB1002501), the

National Natural Science Foundation of China (Grant No. 61673266), and the Fundamental Research Funds for the Central Universities.

References

1. Anund, A., Åkerstedt, T.: Perception of sleepiness before falling asleep. *Sleep Med.* **11**(8), 743–744 (2010)
2. Balandong, R.P., Ahmad, R.F., Saad, M.N.M., Malik, A.S.: A review on EEG-based automatic sleepiness detection systems for driver. *IEEE Access* **6**, 22908–22919 (2018)
3. Bengio, Y., Simard, P.Y., Frasconi, P.: Learning long-term dependencies with gradient descent is difficult. *IEEE Trans. Neural Networks* **5**(2), 157–166 (1994)
4. Guyton, A.C.: *Structure and Function of the Nervous System*. Saunders Limited. (1976)
5. Harland, C.J., Clark, T.D., Prance, R.J.: Remote detection of human electroencephalograms using ultrahigh input impedance electric potential sensors. *Appl. Phys. Lett.* **81**(17), 3284–3286 (2002)
6. Hochreiter, S., Schmidhuber, J.: Long short-term memory. *Neural Comput.* **9**(8), 1735–1780 (1997)
7. Horne, J.A., Baulk, S.D.: Awareness of sleepiness when driving. *Psychophysiology* **41**(1), 161–165 (2004)
8. Jiao, Y., Lu, B.L.: An alpha wave pattern from attenuation to disappearance for predicting the entry into sleep during simulated driving. In: 2017 8th International IEEE/EMBS Conference on Neural Engineering (NER), pp. 21–24 (2017)
9. Jiao, Y., Lu, B.L.: Detecting driver sleepiness from EEG alpha wave during daytime driving. In: 2017 IEEE International Conference on Bioinformatics and Biomedicine (BIBM), pp. 728–731 (2017)
10. Sagberg, F.: Road accidents caused by drivers falling asleep. *Accid. Anal. Prev.* **31**(6), 639–649 (1999)
11. Shabani, H., Mikaili, M., Noori, S.M.R.: Assessment of recurrence quantification analysis (RQA) of EEG for development of a novel drowsiness detection system. *Biomed. Eng. Lett.* **6**(3), 196–204 (2016)
12. Shi, L.C., Lu, B.L.: EEG-based vigilance estimation using extreme learning machines. *Neurocomputing* **102**, 135–143 (2013)
13. Tang, Y.: Deep learning using linear support vector machines. arXiv preprint [arXiv:1306.0239](https://arxiv.org/abs/1306.0239) (2013)
14. Zheng, W.L., Lu, B.L.: A multimodal approach to estimating vigilance using EEG and forehead EOG. *J. Neural Eng.* **14**(2), 26017 (2017)